How to cite: *Angew. Chem. Int. Ed.* **2022,** *61,* e202202014
International Edition: doi.org/10.1002/anie.202202014
German Edition: doi.org/10.1002/ange.202202014

Nitrides Hot Paper

Discovery of Two Polymorphs of TiP_4N_8 Synthesized from Binary Nitrides

Lucien Eisenburger, Valentin Weippert, Carsten Paulmann, Dirk Johrendt, Oliver Oeckler, and Wolfgang Schnick**

Dedicated to Professor Wolfgang Beck on the occasion of his 90th birthday

Abstract: TiP_4N_8 was obtained from the binary nitrides TiN and P_3N_5 upon addition of NH_4F as a mineralizer at 8 GPa and 1400 °C. An intricate interplay of disorder and polymorphism was elucidated by in situ temperature-dependent single-crystal X-ray diffraction, STEM-HAADF, and the investigation of annealed samples. This revealed two polymorphs, which consist of dense networks of PN_4 tetrahedra (degree of condensation $\kappa = 0.5$) and either augmented triangular TiN_7 prisms or triangular TiN_6 prisms for α- and β-TiP_4N_8, respectively. The structures of TiP_4N_8 exhibit body-centered tetragonal (bct) framework topology. DFT calculations confirm the measured band gaps of α- and β-TiP_4N_8 (1.6–1.8 eV) and predict the thermochemistry of the polymorphs in agreement with the experiments.

A variety of group 1 and 2 nitridophosphates has been characterized over the last few decades with silicate-related structural motifs like discrete tetrahedra, layers, or frameworks.[1] An explanation for this abundance of group 1 and 2 nitridophosphates is that P_3N_5, at ambient pressure, readily decomposes above 850 °C under the evolution of N_2.[2] To suppress this degradation, high-pressure high-temperature (HP/HT) synthesis emerged as a viable pathway, following Le Chatelier's principle. The use of stable azides of alkali and alkaline-earth elements proved to be crucial for syntheses. The amount of N_2 from the decomposition of these azides further prevents the decomposition of P_3N_5.

The incorporation of transition metals (*TM*) in nitridic tetrahedral framework structures constitutes a less explored field of research compared to compounds containing group 1 and 2 elements. *TM* bearing compounds are especially interesting given the opportunity to find stable nitrides with suitable band gaps for semiconductor applications like photovoltaics or photocatalysis.[3–5] Although many ternary nitrides with outstanding properties have been predicted by theorists, the synthetic limits still restrict experimental confirmation of these claims.[6,7] Only on a few occasions, the azide-route could be transferred to the synthesis of transition metal nitridophosphates as the respective *TM* azides are either nonexistent or pose serious safety issues due to being explosive.[8] The nitride route, employing the transition metal nitride, was dismissed on many occasions as numerous *TM* nitrides such as ScN, TiN and VN are refractory and unreactive. The requirement to impede the oxidation of the nitride ion and reduction of P or the transition metal constitutes a problem that becomes more severe when the oxidation state of the transition metal increases. Two versatile approaches to gain access to ternary transition metal nitrides have recently been described[1,9,10] and expanded the compositional range of nitridosilicates and -phosphates beyond the well-investigated group 1 and 2 compounds. The cation-exchange approach relies on preformed nitridic networks. For instance, $Ca_2Si_5N_8$ reacts with a $FeCl_2$ melt to yield $Fe_2Si_5N_8$ and $CaCl_2$.[11] Solid-state metathesis of nitridophosphates employs a metal halide and $LiPN_2$ with the formation of lithium halide as a driving force.[12] Both pathways circumvent the formation of stable transition metal phosphides. However, the cation-exchange approach is often limited to the respective nitridic network used in this top-down approach. Solid-state metathesis can be hindered by substantial amounts of Li present. The incorporation of Li beside a heavy transition metal can pose serious problems in terms of structure elucidation.

In our previous studies on the NH_4F mediated HP/HT synthesis, NH_4F has shown its ability to overcome the differing reactivities of Si_3N_4 and P_3N_5 resulting in mixed nitridic networks like the recently described nitridic barylite-($AESiP_3N_7$ AE = Sr, Ba) as well as mica-type compounds

[*] L. Eisenburger, Dr. V. Weippert, Prof. Dr. D. Johrendt, Prof. Dr. W. Schnick
Department of Chemistry, University of Munich
Butenandtstraße 5–13, 81377 Munich (Germany)
E-mail: wolfgang.schnick@uni-muenchen.de
Dr. C. Paulmann
Mineralogisch-Petrographisches Institut
Universität Hamburg
Grindelallee 48, 20146 Hamburg (Germany)
Prof. Dr. O. Oeckler
Institute for Mineralogy, Crystallography and Materials Science, Leipzig University
Scharnhorststraße 20, 04275 Leipzig (Germany)
E-mail: oliver.oeckler@gmx.de

($AESi_3P_4N_{10}(NH)_2$ AE = Mg, $Mg_{0.94}Ca_{0.06}$, Ca, Sr).[9,13] In a similar fashion we employed P_3N_5 and TiN as starting materials although TiN is used as a heat and chemically resistant coating material[14] and despite the tendency of group 4 cations to necessitate the incorporation of oxygen in oxonitridophosphates.[14,15] One may also question if N_2 is a sufficiently strong oxidizing agent at conditions achievable with a multianvil press. Diamond-anvil cell (DAC) experiments resulting in the Ti^{IV}-compounds Ti_3N_4 and TiN_2 from TiN and N_2 had been conducted at 73–75 GPa and 2400 K.[16,17] The oxidizing behavior of nitrogen at elevated pressure could originate from a weakening of the triple bond in N_2 as signaled by the existence of polymeric N exhibiting the crystal structure of black phosphorus or non-molecular N polymorphs.[18–20]

Two polymorphs of the Ti^{IV} nitridophosphate TiP_4N_8, the first ternary compounds of Ti, P and N, were discovered by HP/HT synthesis employing P_3N_5 and TiN as starting materials with the addition of NH_4F as a mineralizing agent and NH_4N_3 as nitrogen source [Eq. 1] at 8 GPa and 1400 °C and subsequent annealing at 700 °C in fused silica ampoules.

$$24\,TiN + 32\,P_3N_5 + 3\,NH_4N_3 \rightarrow 24\,TiP_4N_8 + 4\,NH_3 \quad (1)$$

The HP/HT conditions were achieved by employing a modified Walker-type multianvil press.[21–23] The underlying reason for the success of NH_4F seems to be the reversible element-nitrogen bond cleavage for refractory nitrides that may result in unstable molecular intermediates. In the case of TiN, HF is industrially exploited to convert TiN to the respective Ti fluorides in etching processes.[24] There is no NH_4F with the reaction products, as side reactions with BN, the crucible material, probably occur. HP/HT synthesis yielded β-TiP_4N_8 ($Pmn2_1$, a = 22.9196(5), b = 4.58800(10), c = 8.0970(2) Å, Z = 6, R_1 = 0.0221) as amber crystals (Table 1, S2, S6–8).[25] Ti atoms are coordinated sixfold in TiN_6 triangular prisms with bond lengths $d_{Ti–N}$ ranging from 2.086(3)–2.241(2) Å. The network of PN_4 tetrahedra features all-side vertex-sharing tetrahedra with bond lengths $d_{P–N}$ 1.5998(15)–1.6608(16) Å. The topology of the tetrahedral network can be described as *bct* topology with point symbol 4.6^5 as determined by TOPOS, exhibiting *vierer*, *sechser*, and *achter* rings, according to the nomenclature introduced by Liebau, and a degree of condensation $\kappa = 0.5$ (Figure S1, S2).[26–28]

Structure elucidation of β-TiP_4N_8 by SCXRD led to occupational disorder on Ti sites, an issue that was encountered on datasets of several crystals. STEM-HAADF investigations showed different cation-site occupations for different crystallites ranging from nearly ordered to severely disordered (Figure 1, Table S2, S9–S11). In situ HTSCXRD investigations showed that Ti disorder was eliminated by heating to 600 °C, which became apparent after accounting for limited short-range order by using separate scale factors for reflections with $h = 3n$ and $h \neq 3n$ (Table S2, S12–S14).

Cation ordering was also shown ex situ with samples annealed in silica ampoules at 600 °C. Bond lengths $d_{Ti–N}$ and $d_{P–N}$ are 2.097(4)–2.268(3) Å and 1.605(3)–1.645(3) Å, respectively, at 600 °C and change, as well as bonding angles, only slightly compared to ambient temperatures indicating the rigidity of the network. However, products annealed at 700 °C showed a drastic decrease in crystallite sizes and a change of color (Figure S3).

Ruby-red crystals of α-TiP_4N_8 ($Pmn2_1$, a = 7.6065(2), b = 4.63320(10), c = 7.8601(3) Å, Z = 2, R_1 = 0.0256) were isolated from a sample that was annealed at 700 °C. The structure elucidated by SCXRD (Table S2, S3–S5)[25] is related to that of β-TiP_4N_8 by a cell transformation of 3*a*,*b*,*c* (Table 1, Figure 2 and S4). This also became evident from lattice parameters and reciprocal lattice sections.

The structure of α-TiP_4N_8 strongly resembles that of pseudo-orthorhombic svyatoslavite ($CaAl_2Si_2O_8$, space group $P2_1$).[29,30] As compared to β-TiP_4N_8, α-TiP_4N_8 features no superstructure reflections and a smaller unit cell volume. The orientation of the TiN_x polyhedra is different (Figure 2). Ti is coordinated sevenfold to form TiN_7 augmented triangular prisms enabled by a deformation of the *achter* rings. This leads to a shorter Ti–N distance of 2.540(4) Å (compared to 3.264(4) Å in β-TiP_4N_8). The bond lengths in α-TiP_4N_8 are $d_{Ti–N}$ 2.098(2)–2.540(4) Å and $d_{P–N}$ 1.5758(15)–1.644(2) Å (Figure 3). All observed interatomic distances $d_{P–N}$ agree well with those in comparable compounds.[31,32]

To the best of our knowledge, there is no SCXRD data of a purely nitridic compound featuring Ti^{IV} on a cation site in literature to compare the bonding distances $d_{Ti–N}$ of TiP_4N_8 to.

Table 1: Selected crystallographic information for α- and β-TiP_4N_8 from SCXRD data.

Formula	α-TiP_4N_8	β-TiP_4N_8
molar mass [g mol^{-1}]	283.86	
crystal system	orthorhombic	
space group	$Pmn2_1$ (no. 31)	
lattice parameters [Å]	a = 7.6065(2)	a = 22.9196(5)
	b = 4.63320(10)	b = 4.58800(10)
	c = 7.8601(3)	c = 8.0970(2)
cell volume [Å^3]	277.009(14)	851.44(3)
formula units/ unit cell	2	6
density [g cm^{-3}]	3.403	3.322

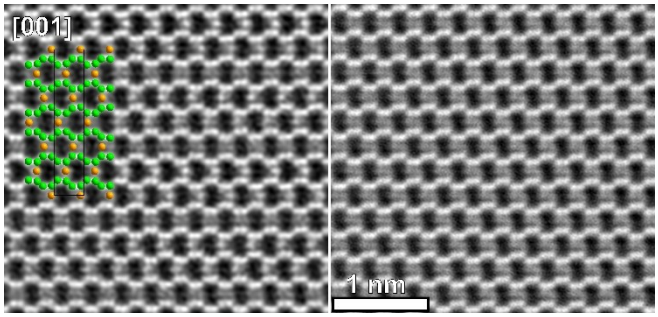

Figure 1. STEM HAADF images of β-TiP_4N_8 before heat treatment along [001]. Almost ordered crystallite on the left and severely disordered on the right. Structure projection of β-TiP_4N_8 with Ti orange, P green, N omitted for clarity.

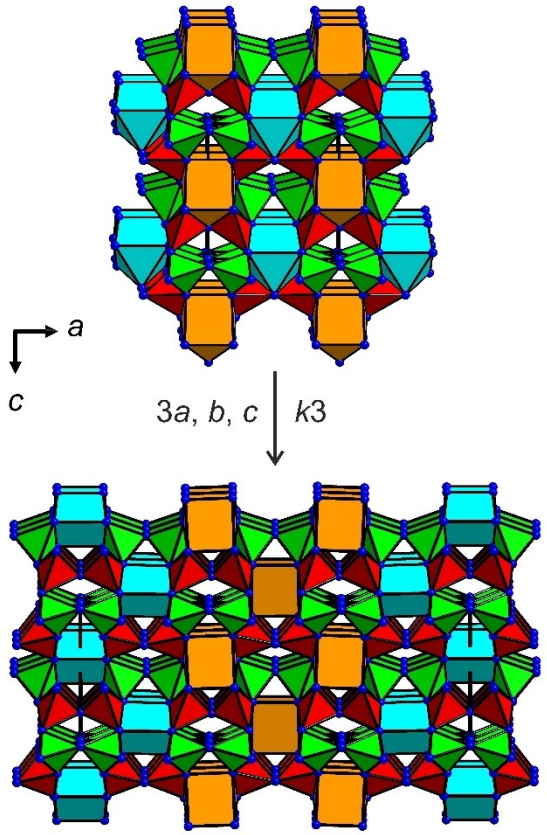

Figure 2. Structure projections of α-TiP_4N_8 (top) and β-TiP_4N_8 (bottom) along ≈[010]. PN_4 tetrahedra in green and red and TiN_x polyhedra in orange and blue, respectively. Different coloring of polyhedra shows different orientations.

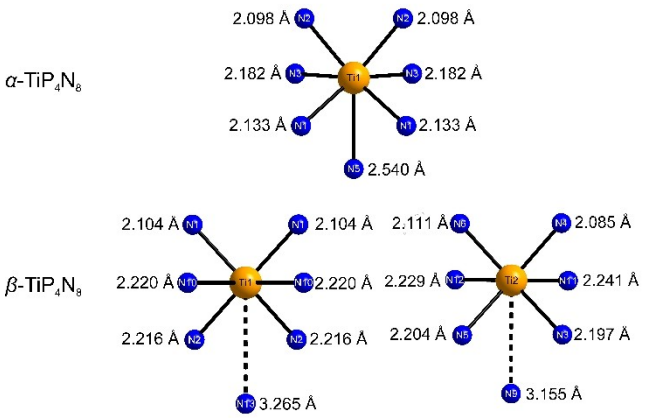

Figure 3. TiN_7 polyhedron in α-TiP_4N_8 (top) and both TiN_6 triangular prisms in β-TiP_4N_8 (bottom): Ti–N bond lengths given next to the corresponding N atom. Dashed Ti–N bonds in β-TiP_4N_8 correspond to the capping atom in α-TiP_4N_8.

Compositional analyses of bulk samples, performed by Rietveld refinements, show TiP_4N_8 as the main constituent of all investigated samples. Minor impurities result from black P, resulting from decomposed P_3N_5, and *h*-BN, which is used as the crucible material (Figure S5 and S6, Table S16).

Energy-dispersive X-ray spectroscopy confirms the composition of Ti:P:N of 1:4:8 supporting the oxidation state of +IV for Ti (Table S15). IR spectroscopy showed no N–H valence modes (Figure S10). BVS calculations of the polymorphs show almost expected values for the bond-valence sums of the individual atom sites for α-TiP_4N_8. For β-TiP_4N_8, the lower coordination numbers lead to smaller values for Ti as well as the affected N sites in contrast to the P sites which again show almost regular values (Table S17, S18). HTPXRD shows thermal stability up to at least 950 °C in Ar atmosphere (Figure S7). HTPXRD with two subsequent heating cycles showed no structural change once β-TiP_4N_8 is converted to α-TiP_4N_8 (Figure S8) DFT calculations of the electronic properties identify both TiP_4N_8 polymorphs as semiconductors with indirect band gaps of 1.35–1.96 eV (α) and 1.21–1.73 eV (β), depending on the exchange-correlation functional used. Figure S12 shows exemplary band structure and density of state plots. Experimental values from reflectance spectra (Figure S11)[33] lead to indirect band gaps of 1.8 and 1.6 eV, respectively, in agreement with the calculated values.

Given the synthesis of β-TiP_4N_8 under HP/HT conditions and subsequent conversion to β-TiP_4N_8 by annealing, it seems obvious that β-TiP_4N_8 is a metastable high-pressure modification. Calculations of the pressure-dependent enthalpy-difference ΔH indicate that β-TiP_4N_8 is only about 8 kJ mol^{-1} less stable than α-TiP_4N_8. However, the pressure dependence of ΔH is very small and the β-modification is predicted to form only at pressures around 50 GPa (Figure 4a), much higher than the synthesis pressure of 8 GPa. To resolve this discrepancy, we have calculated the pressure and temperature dependence of the free energy $G(T,p)$ using the quasi-harmonic approximation (QHA) method.[34,35] For that purpose, the phonon contributions to the free energy F_{ph} at different volumes were calculated, and combined with the electronic energy U^V to obtain the Gibbs free energy using the expression [Eq. (2)]:[36]

$$G(T,p) = \min_{V} \left[U(V) + F_{ph}(T,\ V) + pV\right] \qquad (2)$$

Figure 4b shows the temperature dependence of the Gibbs free energy at different pressures, which reveals that β-TiP_4N_8 is stable above about 1300 K even at zero pressure and that the transition shifts to lower temperatures with increasing pressure. This matches the experimental results much better and predicts that β-TiP_4N_8 is a quenched high-temperature rather than a high-pressure phase. Finally, we calculated the energy barrier between the polymorphs using the climbing nudged elastic band (Cl-NEB) method.[37] Figure 5 shows the NEB energy profile and a cutout of the structure at the transition state. Titanium has four short (2.01–2.03 Å) and four long (2.75–2.87 Å) Ti–N contacts. The position is almost symmetric between the two distant nitrogen atoms (3.12–3.37 Å), one of which becomes the capping atom of the TiN_7 polyhedron in α-TiP_4N_8 (Figure 3).

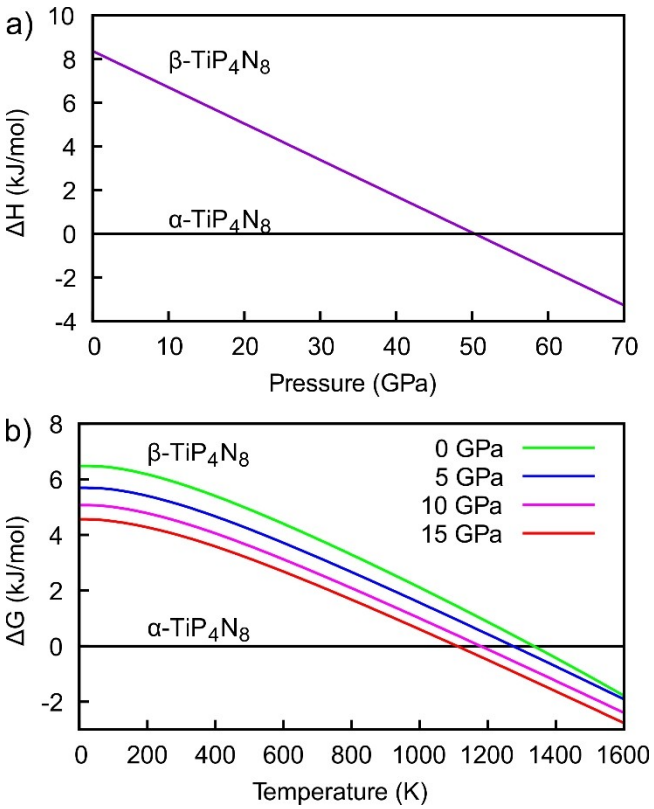

Figure 4. a) Enthalpy difference ΔH between β- and α-TiP_4N_8 with increasing pressure. b) Temperature dependence of the Gibbs free energy difference ΔG at different pressures.

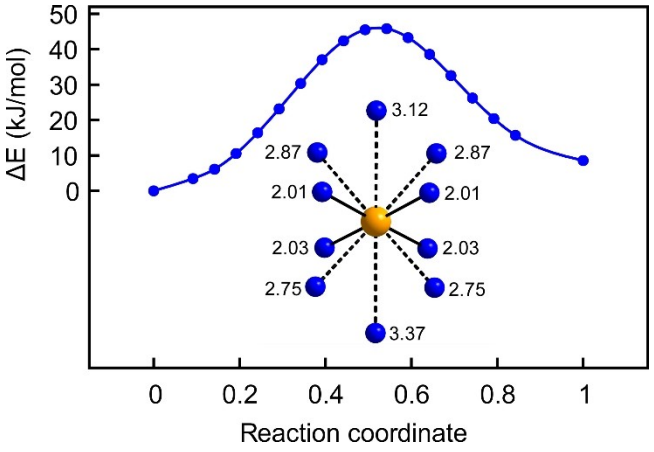

Figure 5. Energy barrier of the α-TiP_4N_8 to β-TiP_4N_8 transition and the coordination of titanium at the transition state with d_{Ti-N} (in Å) adjacent to N atoms.

Summing up, the first Ti-nitridophosphate, TiP_4N_8, was synthesized by HT/HP synthesis with NH_4F as a mineralizing agent. A combination of STEM-HAADF, in situ HTSCXRD investigations and annealing experiments revealed two polymorphs of TiP_4N_8. The occupational disorder of Ti almost vanished at 600 °C resulting in β-TiP_4N_8. Further heating leads to a transformation to α-TiP_4N_8. DFT calculations including temperature-dependent phonon contributions indicate that β-TiP_4N_8 is a metastable high-temperature polymorph. The presented synthesis of the first Ti^{IV}-nitridophosphate from binary nitrides marks a starting point to straightforward syntheses of a multitude of ternary transition metal nitrides. Given the band gaps of α- and β-TiP_4N_8 both compounds absorb light in the visible part of the spectrum. Band gaps are comparable to those of CdTe, 1.513 eV, and GaAs, 1.423 eV.[38,39] It is most likely that the NH_4F-assisted approach can be adapted for other *TM* nitrides as well, diversifying the compositional range and variability of crystal structures in nitrides, significantly. The present results indicate that the oxidative potential of N in the pressure and temperature range of a multianvil press is sufficient to prevent the formation of *TM* phosphides from reactions of the binary nitrides.

Acknowledgements

Financial support by the Deutsche Forschungsgemeinschaft DFG (projects SCHN 377/7, SCHN 377/18-1 and OE 513/6-1) as well as under Germany's Excellence Strategy—EXC 2089/1—390776260 is gratefully acknowledged. We thank Dr. Peter Mayer for single-crystal data collection and Lisa Gamperl for SEM investigations. We are also indebted to Daniel Günther, Tobias Lindemann and Lennart Staab for the collection of HTSCXRD data. Parts (project I-20191265) of this research were carried out at PETRA III at DESY, a member of the Helmholtz Association. We would like to thank Martin Tolkiehn for his assistance in using beamline P24. The authors gratefully acknowledge the computational and data resources provided by the Leibniz Supercomputing Centre (www.lrz.de). Open Access funding enabled and organized by Projekt DEAL.

Conflict of Interest

The authors declare no conflict of interest.

Data Availability Statement

The data that support the findings of this study are available in the supplementary material of this article.

Keywords: Density Functional Theory · Disordered Compounds · High-Pressure Chemistry · Nitrides · Titanium

[1] S. D. Kloß, W. Schnick, *Angew. Chem. Int. Ed.* **2019**, *58*, 7933–7944; *Angew. Chem.* **2019**, *131*, 8015–8027.
[2] S. Horstmann, E. Irran, W. Schnick, *Angew. Chem. Int. Ed. Engl.* **1997**, *36*, 1873–1875; *Angew. Chem.* **1997**, *109*, 1938–1940.
[3] I. Dincer, C. Zamfirescu, *Sustainable Hydrogen Production*, Elsevier, Amsterdam, **2016**, pp. 309–391.
[4] A. Fuertes, *J. Mater. Chem.* **2012**, *22*, 3293–3299.

[5] R. S. Ningthoujam, N. S. Gajbhiye, *Prog. Mater. Sci.* **2015**, *70*, 50–154.
[6] A. L. Greenaway, C. L. Melamed, M. B. Tellekamp, R. Woods-Robinson, E. S. Toberer, J. R. Neilson, A. C. Tamboli, *Annu. Rev. Mater. Res.* **2021**, *51*, 591–618.
[7] W. Sun, C. J. Bartel, E. Arca, S. R. Bauers, B. Matthews, B. Orvañanos, B. R. Chen, M. F. Toney, L. T. Schelhas, W. Tumas, J. Tate, A. Zakutayev, S. Lany, A. M. Holder, G. Ceder, *Nat. Mater.* **2019**, *18*, 732–739.
[8] F. J. Pucher, F. W. Karau, J. Schmedt auf der Günne, W. Schnick, *Eur. J. Inorg. Chem.* **2016**, 1497–1502.
[9] L. Eisenburger, O. Oeckler, W. Schnick, *Chem. Eur. J.* **2021**, *27*, 4461–4465.
[10] L. Eisenburger, V. Weippert, O. Oeckler, W. Schnick, *Chem. Eur. J.* **2021**, *27*, 14184–14188.
[11] P. Bielec, O. Janka, T. Block, R. Pöttgen, W. Schnick, *Angew. Chem. Int. Ed.* **2018**, *57*, 2409–2412; *Angew. Chem.* **2018**, *130*, 2433–2436.
[12] S. D. Kloß, O. Janka, T. Block, R. Pöttgen, R. Glaum, W. Schnick, *Angew. Chem. Int. Ed.* **2019**, *58*, 4685–4689; *Angew. Chem.* **2019**, *131*, 4733–4737.
[13] L. Eisenburger, P. Strobel, P. J. Schmidt, T. Bräuniger, J. Wright, E. L. Bright, C. Giacobbe, O. Oeckler, W. Schnick, *Angew. Chem. Int. Ed.* **2022**, *61*, e202114902; *Angew. Chem.* **2022**, *134*, e202114902.
[14] E. Santecchia, A. M. S. Hamouda, F. Musharavati, E. Zalnezhad, M. Cabibbo, S. Spigarelli, *Ceram. Int.* **2015**, *41*, 10349–10379.
[15] S. D. Kloß, S. Wandelt, A. Weis, W. Schnick, *Angew. Chem. Int. Ed.* **2018**, *57*, 3192–3195; *Angew. Chem.* **2018**, *130*, 3246–3249.
[16] V. S. Bhadram, D. Y. Kim, T. A. Strobel, *Chem. Mater.* **2016**, *28*, 1616–1620.
[17] V. S. Bhadram, H. Liu, E. Xu, T. Li, V. B. Prakapenka, R. Hrubiak, S. Lany, T. A. Strobel, *Phys. Rev. Mater.* **2018**, *2*, 011602.
[18] A. F. Goncharov, E. Gregoryanz, H. K. Mao, Z. Liu, R. J. Hemley, *Phys. Rev. Lett.* **2000**, *85*, 1262.
[19] D. Laniel, B. Winkler, T. Fedotenko, A. Pakhomova, S. Chariton, V. Milman, V. Prakapenka, L. Dubrovinsky, N. Dubrovinskaia, *Phys. Rev. Lett.* **2020**, *124*, 216001.
[20] C. Ji, C. Ji, A. A. Adeleke, L. Yang, B. Wan, H. Gou, Y. Yao, B. Li, Y. Meng, J. S. Smith, V. B. Prakapenka, W. Liu, G. Shen, W. L. Mao, H. K. Mao, *Sci. Adv.* **2020**, *6*, 9206–9209.
[21] D. Walker, *Am. Mineral.* **1991**, *76*, 1092–1100.
[22] D. Walker, M. A. Carpenter, C. M. Hitch, *Am. Mineral.* **1990**, *75*, 1020–1028.
[23] H. Huppertz, *Z. Kristallogr.* **2004**, *219*, 330–338.
[24] Y. Lee, S. M. George, *Chem. Mater.* **2017**, *29*, 8202–8210.
[25] Deposition Numbers 2121161, 2121162, 2121163 and 2121164 contain the supplementary crystallographic data for this paper. These data are provided free of charge by the joint Cambridge Crystallographic Data Centre and Fachinformationszentrum Karlsruhe Access Structures service.
[26] W. A. Dollase, C. R. Ross, *Am. Mineral.* **1993**, *78*, 627–632.
[27] V. A. Blatov, A. P. Shevchenko, D. M. Proserpio, *Cryst. Growth Des.* **2014**, *14*, 3576–3586.
[28] F. Liebau, *Structural Chemistry of Silicates*, Springer, Berlin, Heidelberg, **1985**.
[29] S. V. Krivovichev, E. P. Shcherbakova, T. P. Nishanbaev, *Can. Mineral.* **2012**, *50*, 585–592.
[30] Y. Takéuchi, N. Haga, J. Ito, *Z. Kristallogr. New Cryst. Struct.* **1973**, *137*, 380–398.
[31] S. Wendl, L. Eisenburger, P. Strobel, D. Günther, J. P. Wright, P. J. Schmidt, O. Oeckler, W. Schnick, *Chem. Eur. J.* **2020**, *26*, 7292–7298.
[32] S. Vogel, A. T. Buda, W. Schnick, *Angew. Chem. Int. Ed.* **2018**, *57*, 13202–13205; *Angew. Chem.* **2018**, *130*, 13386–13389.
[33] J. Tauc, R. Grigorovici, A. Vancu, *Phys. Status Solidi* **1966**, *15*, 627–637.
[34] M. T. Dove, *Introduction to Lattice Dynamics*, Cambridge University Press, Cambridge, **1993**.
[35] R. P. Stoffel, C. Wessel, M. W. Lumey, R. Dronskowski, *Angew. Chem. Int. Ed.* **2010**, *49*, 5242–5266; *Angew. Chem.* **2010**, *122*, 5370–5395.
[36] A. Togo, I. Tanaka, *Scr. Mater.* **2015**, *108*, 1–5.
[37] K. J. Caspersen, E. A. Carter, *Proc. Natl. Acad. Sci. USA* **2005**, *102*, 6738–6743.
[38] G. Fonthal, L. Tirado-Mejía, J. I. Marín-Hurtado, H. Ariza-Calderón, J. G. Mendoza-Alvarez, *J. Phys. Chem. Solids* **2000**, *61*, 579–583.
[39] J. S. Blakemore, *J. Appl. Phys.* **1982**, *53*, R123.

Manuscript received: February 6, 2022
Accepted manuscript online: February 18, 2022
Version of record online: February 28, 2022